doi:10.3166/acsm.40.17-24 © Lavoisier, Paris

Ann. Chim. Sci. Mat., 2016, 40 (1-2), pp. 17-24

MICROSTRUCTURE AND CORROSION BEHAVIOUR OF COBALT-MOLYBDENUM COATINGS ELECTRODEPOSITED ON PURE COBALT

Vincent VIGNAL[a], Halina KRAWIEC[b], Paulina ERAZMUS-VIGNAL[a], Michal LATKIEWICZ[b]

[a] Laboratoire de Interdisciplinaire Carnot de Bourgogne, UMR 6303 CNRS - Université Bourgogne Franche-Comté, BP 47870, 21078 Dijon cedex, France.
[b] AGH University of Science and Technology, Faculty of Foundry Engineering, ul. Reymonta 23, 30-059 Krakow, Poland.

Abstract - Electrodeposition is a versatile route to produce new nanocrystalline alloys. Only a few studies concern the corrosion behaviour of these nanocrystalline alloys. In the present paper, the physical-chemical properties of Co-Mo coatings electrodeposited on pure cobalt are investigated by means of field-emission scanning electron microscopy coupled with energy dispersive spectroscopy (FE-SEM/EDS), optical profilometry and microhardness tests. The influence of potential applied during electrodeposition is discussed. The corrosion behaviour of these coatings is then studied in the Ringer's solution at 25 °C. Obtained results are analyzed considering the physical-chemical properties of coatings.

Résumé - Microstructure et comportement en corrosion de revêtements Co-Mo électrodéposés sur du cobalt pur. L'électrodéposition est une méthode simple pour produire des alliages nano cristallisés. Dans cet article, les propriétés physico-chimiques de revêtements Co-Mo électrodéposés sur du cobalt pur sont étudiées à l'aide de la microscopie électronique à balayage à effet de champ couplé à une microsonde X (MEB-EC/EDS), de la profilométrie optique et de tests de microdureté. L'influence du potentiel appliqué pendant l'électrodéposition est discutée. Le comportement en corrosion des ces revêtements est ensuite étudié dans une solution de Ringer à 25 °C. Les résultats obtenus sont analysés en tenant compte des propriétés physico-chimiques des revêtements.

1. INTRODUCTION

Electrodeposition is a versatile route to produce new nanocrystalline alloys [1-2]. Numerous studies [3-8] have shown that these new nanocrystalline alloys have excellent mechanical properties. Indeed, they can undergo severe plastic deformation and they have high hardness and good resistance to wear. Other studies have shown that these alloys also have specific physical-chemical properties (such as magnetic, electronic, catalytic and optical properties). Therefore, they can find applications in many industrial sectors: biology, energy, nanotechnologies, aerospace… [9]. Electrodeposited nanocrystalline alloys can also replace other materials or coatings for which elaboration processes are polluting or/and dangerous for health [10].

Tirés-à-part: V. VIGNAL, ICB, UMR 6303 CNRS – Universite Bourgogne Franche-Comte, 9 Avenue Alain Savary, BP 47870, 21078 Dijon Cedex, France.

Synthesis process and the nanostructure of these alloys are generally well known and controlled [11-13]. By contrast, only a few studies [14-18] concern their corrosion behaviour. These studies have generally been conducted at the macroscale using classical techniques. Local electrochemical techniques have only been used in ref. [14]. They have compared the behaviour of nano- and microcrystalline alloys (both having the same chemical composition). Nanocrystalline alloys exhibit systematically higher corrosion resistance than alloys with coarse grains. Some assumptions have been proposed to explain these results: role of the grain boundaries, residual stresses... However, the corrosion behaviour of nanocrystalline alloys is not well understood yet.

In the present paper, the microstructure and mechanical properties of Co-Mo coatings electrodeposited on pure cobalt are investigated by means of optical profilometry, field-emission scanning electron microscopy coupled with energy dispersive spectroscopy (FE-SEM/EDS), microhardness tests and X-ray photoelectron spectroscopy (XPS). The influence of potential applied during electrodeposition is discussed. The corrosion behaviour of these coatings is then studied in the Ringer's solution at 25 °C.

2. EXPERIMENTAL CONDITIONS

Co samples (99.99%, delivered by Goodfellow) were first mechanically ground with emery papers (down to 4000 grit), cleaned in ethanol under ultrasonics for 5 minutes and then dried in air. Co samples were partly coated with acrylic painting (from Vishay). Co-Mo coatings were then electrodeposited at various applied potentials under stirring (~230 rpm). The aqueous solution used for electrodeposition is 0.2M $CoSO_4 \cdot 7H_2O$ + 0.02M $Na_2MoO_4 \cdot 2H_2O$ + 0.5M H_3BO_3 + 0.2M $C_6H_5Na_3O_7$. The solution pH and temperature are 4.9 and 25 °C, respectively. Electrodeposition was carried out for 5 minutes. A saturated calomel reference (SCE) was used in these experiments. After electrodeposition, samples were cleaned in distilled water and then in acetone under ultrasonics for 1 minute. During this operation, the acrylic painting was totally removed. Samples were again cleaned in distilled water for few seconds. The substrate was then locally exposed to ambient air (non-coated zone).

To measure the thickness of coatings line scans (2 mm in length by step of 0.5 µm) were plotted through the interface between the coated and non-coated zones. This was done by means of optical profilometry (AltiSurf 500 white light equipment from Cotec having a dynamic range of 50 nm–300 µm).

On the other hand, a field-emission type Scanning Electron Microscope (JEOL 6400F) with an integrated electron dispersion spectrometer (FE-SEM/EDS) was used to determine the chemical composition and morphology of coatings. The chemical composition of the coating deposited at -1.2 V vs. SCE was also determined using XPS. The equipment was a SIA 100 Cameca Riber apparatus and a nonmonochromated Al Kα line (energy of 1486.6 eV, power of 300 W and X-ray beam diameter of 200 µm). A Mac 2 semi-imaging spectrometer was used with a resolution of 1.3 eV (width of Ag $3d_{5/2}$ level). C1s peak from pollution (285 eV) was considered for the energy calibration. During measurements the residual pressure of the analysis chamber was maintained below 10^{-7} Pa. Spectra were treated with the Casa software package and ionization cross-sections from Landau were used in order to quantify the semi-empirical relative sensitivity factors. Depth profiling was performed using 500 eV argon ions. The sputtering rate was measured on a pure SiO_2 thermal oxide (2.74 nm/min).

Microhardness tests were carried out on coatings with an applied load of 10 gf (gram-force) using low-load Vickers micro-indentation hardness testing (Micromet 5114 with Omninet image acquisition and analysis software from Buehler).

Local polarisation curves were plotted at a potential scan rate of 1 mV/s in the Ringer's solution at 25 °C (pH adjusted to 7.2 by adding NaOH). The experiments were performed using the electrochemical microcell technique [19-21], capillaries with a diameter of 150 µm and a PGSTAT302 AUTOLAB potentiostat/ galvanostat. No prior cathodic polarisation was applied to the system. All potentials were measured vs. silver / silver chloride reference electrode (Ag/AgCl) and the counter electrode was made of platinum wire.

3. EXPERIMENTAL RESULTS AND DISCUSSION

Cyclic voltammogramms were first plotted on Pt substrate in 0.2M $CoSO_4 \cdot 7H_2O$ + 0.02M $Na_2MoO_4 \cdot 2H_2O$ + 0.5M H_3BO_3. 15 cycles were plotted at a potential scan rate of 100 mV/s, *figure 1*. The oxidation peak P1 visible at roughly -0.08 V vs. SCE on the forward scan may correspond to the oxidation of sulphur species present in the solution according to reactions (1) and (2):

$$2SO_4^{2-} + 4H^+ + 2e \leftrightarrow S_2O_6^{2-} + 2H_2O \text{ standard potential } E_0 = = -0.22 \text{ V vs. NHE} \quad (1)$$

$$S_2O_6^{2-} + 4H^+ + 2e \leftrightarrow 2H_2SO_3 \text{ standard potential } E_0 = 0.564 \text{ V vs. NHE} \quad (2)$$

In addition, Co deposited at the specimen surface can also be dissolved within this potential range [22]. Two reduction peaks are also visible on the reverse scan: the peak P2 at -0.9 V vs. SCE is associated to the reduction of molybdates and the peak P3 at -1.13 V vs. SCE is associated to the reduction of Co ions [21]. Previous works [22-23] showed that molybdenum can easily be oxidized to form molybdenum oxide (MoO_2) which may block the deposition of Mo at the specimen surface. It may also hinder the Co reduction on the electrode surface, but it does not block it. In the cathodic domain, the hydrogen evolution reaction (reaction 3) and water dissociation (reaction 4) can also take place. An intense hydrogen release can induce local dissolution of the coating when polarization is stopped (due to the presence of hydrogen bubbles at the specimen surface) and can also prevent the Co–Mo crystallization [22].

$$2H^+ + 2e^- \rightarrow H_2, \text{ standard potential } E_0 = 0 \text{ V vs. NHE} \quad (3)$$

$$2H_2O + 2e^- \rightarrow H_2 + 2OH^-, \text{ standard potential } E_0 = -0.828 \text{ V vs. NHE} \quad (4)$$

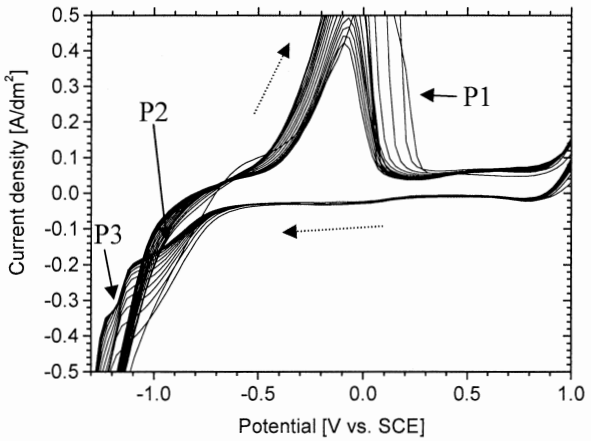

Figure 1. Cyclic voltammogramms (100 mV/s) on Pt substrate in 0.2M $CoSO_4 \cdot 7H_2O$ + 0.02M $Na_2MoO_4 \cdot 2H_2O$ + 0.5M H_3BO_3.

3.1. Physical-chemical properties of coatings

According to the results obtained on Pt substrate, electrodeposition of Co-Mo coatings on Co samples was performed at applied potentials of -0.9, -1, 1.1, -1.2 and -1.3 V vs. SCE. Citrates (0.2M $C_6H_5Na_3O_7$) were added in the solution to hinder the formation of cracks and to promote the deposition of coherent and homogeneous coatings [23]. After electrodeposition, the coatings were analysed by means of optical profilometry (thickness), FE-SEM/EDS (chemical composition and morphology) and microindentation tests (hardness). The presence of defects (cracks or pores for example) was also investigated by means of FE-SEM.

Coatings with a thickness greater than 1.5 µm (applied potentials of -1.2 and -1.3 V vs. SCE in *table I*) were analysed by means of FE-SEM/EDS at 15 kV (classical conditions). By contrast, thin coatings (applied potentials of -0.9, -1 and -1.1 V vs. SCE) were analysed at 5 kV to minimize the volume irradiated. The penetration depth of the indenter into the materials was also calculated geometrically from the values of the indent size (in the range of 6-8 µm) and the angle between opposite faces of the Vickers indenter (of 136°). The penetration depth was close to 1.2 µm. Hardness measurements on thin coatings (thickness less than 1.5 µm) were then affected by the substrate. Therefore, only results on thick coatings (applied potentials of -1.2 and -1.3 V vs. SCE in *table I*) were interpreted.

Table I. Physical-chemical properties of Co-Mo coatings deposited on Co samples at various applied potentials. FE-SEM/EDS analysis performed at (*) 5kV and (**) 15 kV. Numbers in brackets represent the standard deviation.

Applied potential (V vs. SCE)	Thickness (µm)	Hardness (HV_{10})	Chemical composition (at.%) - XPS			Chemical composition (at.%) – FE-SEM/EDS		
			O	Co	Mo	O	Co	Mo
-0.9*	/	/	/	/	/	2.6	97.4	0
-1*	0.34 (0.09)	375 (13)	/	/	/	6	90.8	3.2
-1.1*	1.18 (0.13)	388 (4)	/	/	/	6.1	76.4	17.6
-1.2**	1.82 (0.26)	422 (26)	7.2	68.4	22.1	5	73.9	21.1
-1.3**	2.26 (0.04)	477 (3)	/	/	/	4.8	75.3	19.8

The thickness of coatings was found to increase with increasing applied potential (from roughly 0.3 µm at -1 V vs. SCE up to roughly 2.3 µm at -1.3 V vs. SCE), *table I*. Note that it was impossible to measure the thickness of the coating deposited at -0.9 V vs. SCE. In addition, the coatings were found to be significantly harder (values around 450 HV_{10}) than the substrate (values of about 260 HV_{10}). This was explained by the fact that the Co-Mo coating is nanostructured (XRD results not shown here) whereas the Co substrate has a coarse microstructure.

The oxygen content in the coating was systematically low (about 5 at.% in *table I*). This suggests that these coatings are mainly composed of species in the metallic form. This was confirmed from XPS measurements performed on the coating deposited at -1.2 V vs. SCE (*figure 2*). Both oxide-based compounds and metallic elements are detected in the absence of sputtering prior to XPS measurements (t = 0 min in *figure 2*). After 1 minute of sputtering (removed thickness of about 2.7 nm, t = 1 min in *figure 2*), oxide-based compounds are almost not detected, indicating that these compounds were mainly located at the extreme surface. This result demonstrates that the coating is covered by a native passive film and that the coating bulk is mainly composed of metallic Co and Mo.

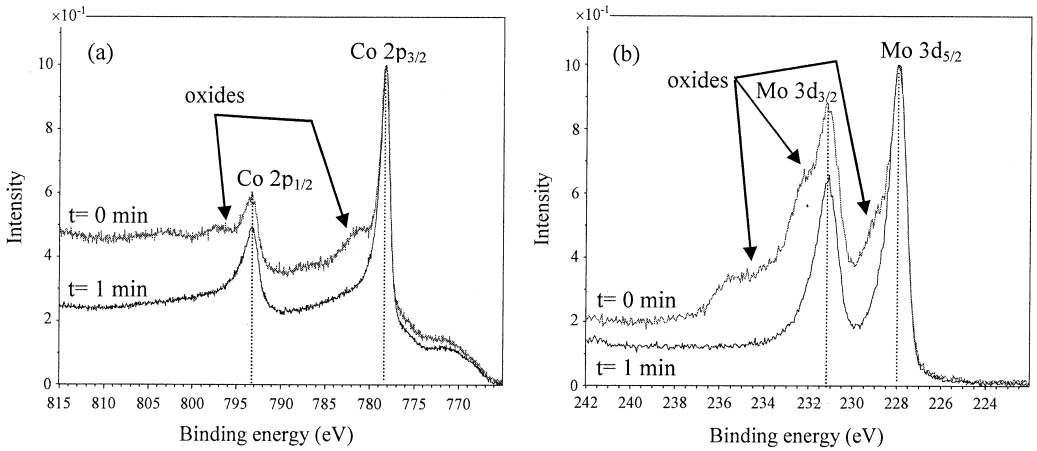

Figure 2. XPS spectra of (a) Co 2p and (b) Mo 3d levels derived from XPS measurements on the coating deposited at -1.2 V vs. SCE. XPS measurements were performed without sputtering (t = 0 min) and after 1 minute of sputtering (t = 1 min).

The molybdenum content in the coating increases sharply with increasing applied potential (0 at.% at -0.9 V vs. SCE up to around 20 at.% at -1.2 V vs. SCE. From an applied potential of -1.2 V vs. SCE, the molybdenum content is more-or-less constant (around 20 at.%, *table I*) and does not depend on the applied potential value. These results show that the molybdenum content cannot exceed a limit. It is interesting to note that similar results (contents in oxygen, cobalt and molybdenum) were obtained both from FE-SEM/EDS and XPS (*table I*). This tends to validate the obtained results.

Figures 3(a)-(d) show FE-SEM images of the surface of coatings. At an applied potential of -1 V vs. SCE, the coating was found to be locally extremely thin (sites located by circles in *figure 3(a)*). Except in these sites, the coating appears coherent and homogeneous. From -1.1 V vs. SCE (*figures 3(b)-(d)*), islands are observed. FE-SEM/EDS analysis performed in these islands show that they have the same chemical composition as the coating:
point A in *figure 3(d)* : 5.8 at.% O, 76.8 at.% Co and 19.1 at.% Mo
point B in *figure 3(d)* : 4.1 at.% O, 74.2 at.% Co and 19.9 at.% Mo
The equivalent diameter of these islands increases with increasing applied potential. It is in the range of 0.8 µm at -1.1 V vs. SCE (*figure 3(b)*), 2 µm at -1.2 V vs. SCE (*figure 3(c)*) and 2-8 µm at -1.3 V vs. SCE (*figure 3(d)*). This suggests that the way of growth of this Co/Mo coating is of Stranski-Krastanov mode. The mode follows a two step process. Initially the coating grows in a layer-by-layer fashion on the substrate. Beyond a critical layer thickness, which depends on strain and on the chemical potential of the coating, growth continues through the nucleation and coalescence of islands. In the case of Co/Mo the critical thickness seems to be around 1 µm (applied potential of -1.1 V vs. SCE).

At -1.3 V vs. SCE, numerous cracks were observed in the coating (*figure 3(d)*). It is well known that residual stresses develop in the coatings during deposition. The presence of numerous cracks suggests that tensile stresses generated in this coating (deposited at -1.3 V vs. SCE) exceed the elastic limit and cause cracking. Under these conditions, the presence of citrates in the solution does not assure coherent homogeneous coatings.

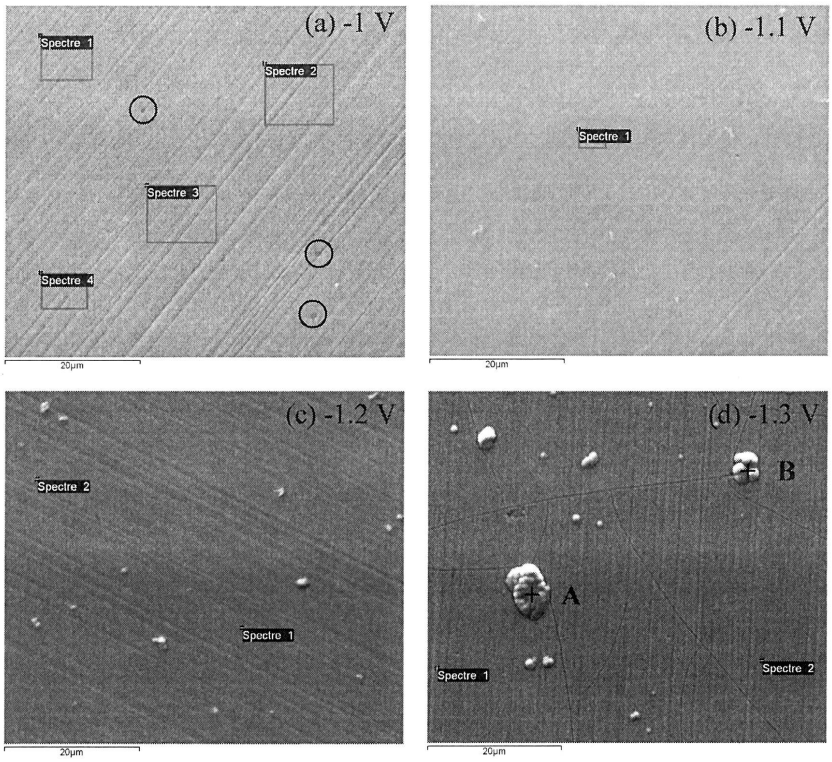

Figure 3. FE-SEM images of the Co-Mo coating deposited on pure Co at various applied potentials: (a) -1 V vs. SCE, (b) -1.1 V vs. SCE, (c) -1.2 V vs. SCE and (d) -1.3 V vs. SCE.

Electrochemical measurements were then performed on the coating deposited at -1.2 V vs. SCE. Indeed, this coating is homogeneous in terms of thickness and chemical composition, is nanostructured (presence of nanograins), contains a large amount of molybdenum (about 20 at.%) and is free of cracks.

3.2. Corrosion behaviour of coatings

Figures 4(a) and 4(b) show the evolution of the open circuit potential (OCP) vs. time and the polarisation curves of the substrate (pure cobalt) and the coating deposited at -1.2 V vs. SCE in the Ringer's solution at 25 °C (pH = 7.2). The OCP of the substrate fluctuates and drops sharply (drop of about 100 mV within 1500 seconds of immersion), *figure 4(a)*. By contrast, the OCP of the coating increases slightly to reach quickly a steady state (values around -570 mV vs. Ag/AgCl).

The substrate (pure cobalt) exhibits an extremely narrow passive range defined by a current density in the range of 3-4 $\mu A/cm^2$ (grey curves in *figure 4(b)*). Pitting corrosion is observed from an applied potential around -0.3 V vs. Ag/AgCl. The current density in the cathodic branch of the coating (black curves in *figure 4(b)*) is significantly lower than on the substrate. The oxygen reduction reaction is maybe hindered by the presence of molybdenum in the coating. A plateau is again observed in the anodic branch of the coating, but the current density associated to this plateau (of about 100 $\mu A/cm^2$) was roughly two orders of magnitude greater than on the substrate. This shows that the corrosion resistance of the coating deposited at -1.2 V vs. SCE is lower than that of pure Co.

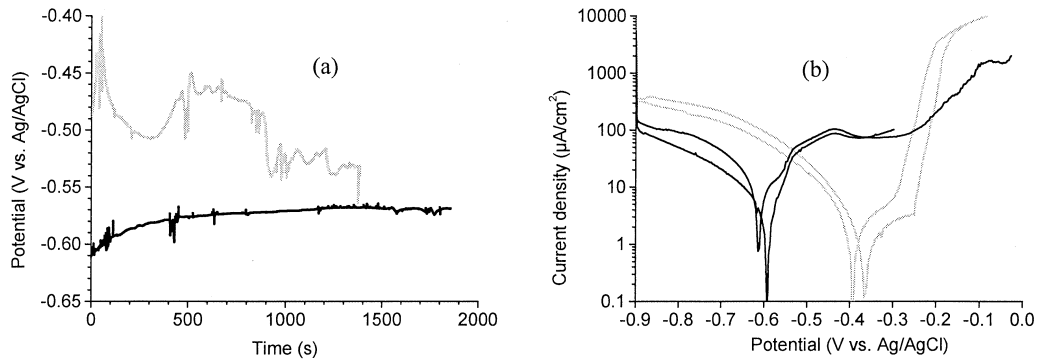

Figure 4. Electrochemical measurements (capillary diameter of 150 μm) on the substrate (grey curves) and the coating deposited at -1.2 V vs. SCE (black curves) in the Ringer's solution at 25 °C with pH = 7.2: (a) open circuit potential vs. time plots and (b) local polarisation curves (1 mV/s).

4. CONCLUSIONS

The following conclusions can be drawn:
(1) The chemical composition and thickness of the Co-Mo coating closely depends on the potential applied during electrodeposition. The highest values of the thickness and molybdenum content are roughly 2.3 μm and 21at.%, respectively
(2) Islands with the same chemical composition as the coating are observed at the specimen surface (Stranski-Krastanov mode)
(3) For the highest applied potential value (-1.3 V vs. SCE) cracks are observed in the Co-Mo coating (tensile stresses exceed the elastic limit)
(4) The Co-Mo coating is harder than the Co substrate (nanostructured coating)
(5) The Co-Mo coating is covered by a native passive film
(6) The corrosion resistance of the coating is lower than that of pure Co.

5. REFERENCES

[1] C. Suryanarayana, C.C. Koch, Hyperfine Interactions 130 (1-4) (2000) 5–44.
[2] M. Bhardwaj, K. Balani, R. Balasubramaniam, S. Pandey, A. Agarwal, Surface Engineering 27 (9) (2011) 642-648.
[3] A.A. Karimpoor, U. Erb, K.T. Aust, G. Palumbo, Scripta Materialia 49 (7) (2003) 651–656.
[4] P. Cavaliere, International Journal of Fatigue 31 (10) (2009) 1476–1489.
[5] L.P. Bicelli, B. Bozzini, C. Mele, L. D'Urzo, International Journal of Electrochemical Science 3 (4) (2008) 356-408.
[6] Y.M. Wang, S. Cheng, Q.M. Wei, E. Ma, T.G. Nieh, A. Hamza, Scripta Materialia 51 (11) (2004) 1023–1028.
[7] L. Wang, Y. Gao, T. Xu, Q. Xue, Materials Chemistry and Physics 99 (1) (2006) 96–103.
[8] D.H. Jeong, F. Gonzalez, G. Palumbo, K.T. Aust, U. Erb, Scripta Materialia 44 (3) (2001) 493–499.
[9] M.C. Roco, C.A. Mirkin, M.C. Hersam, WTEC Panel Report on 'Nanotechnology Research Directions for Societal Needs in 2020: Retrospective and Outlook', Chapter 11, pp. 361-388, September 2010, Springer Editions.

[10] R.A. Prado, D. Facchini, N. Mahalanobis, F. Gonzalez, G. Palumbo, Proceedings of the Department of Defense Corrosion Conference, 10-14 august 2009 Gaylord National, Washington DC (USA).
[11] B.Y.C. Wu, Degree of Master of Science in Materials Science and Engineering, University of Toronto, Canada (2002).
[12] M. Spasojević, L. Ribić-Zelenović, A. Maričić, Science of Sintering 43 (3) (2011) 313-327.
[13] L.D. Rafailović, D.M. Minic, Hemijska Industrija 63 (5a) (2009) 557–569.
[14] F. Contu, B. Elsener, H. Bohni, Corrosion Science 47 (8) (2005) 1863-1875.
[15] A. Heidari, N. Heidari, F.K. Jahromi, R. Amiri, M. Zeinalkhani, F. Ghorbani, A. Piri, M. Ghorbani, International Journal of Scientific & Engineering Research 3 (3) (2012) 360-363.
[16] S.H. Kim, K.T. Aust, U. Erb, F. Gonzalez, G. Palumbo, Scripta Materialia 48 (9) (2003) 1379–1384.
[17] D. Cheng, V.L. Tellkamp, C.J. Lavernia, E.J. Lavernia, Annals of Biomedical Engineering 29 (9) (2001) 803–809.
[18] M.S. Cheraghi, S.R. Allahkaram, N. Towhidi, S.K. Khonsari, T. Rabizadeh, Proceedings of the Nanotechnology Materials and Devices Conference (NMDC), 2011 IEEE, pp. 228-231.
[19] H. Krawiec, V. Vignal, E. Finot, O. Heintz, R. Oltra, Metallurgical and Materials Transactions A-Physical Metallurgy and Materials Science 35 (11) 3515-3521.
[20] H. Krawiec, V. Vignal, R. Akid, Surface and Interface Analysis 40 (3-4) 315-319.
[21] H. Krawiec, V. Vignal, H. Amar, P. Peyre, Electrochimica Acta 56 (26) 9581-9587.
[22] Y. Messaoudi, N. Fenineche, A. guittoum, A. Azizi, G. Schmerber, A. Dinia, Journal of Materials Science : Materials in Electronics 24 (8) (2013) 2962-2969.
[23] E. Gomez, E. Pellicer, E. Valles, Journal of Electroanalytical Chemistry 556 (2003) 137-145.

(Article reçu le 01/10/2015, sous forme définitive le 07/01/2016).